Fast Explicit and Unconditionally Stable FDTD Method for Electromagnetic Analysis

Jin Yan, *Graduate Student Member, IEEE*, and Dan Jiao, *Fellow, IEEE*

***Abstract*— In this paper, a fast explicit and unconditionally stable finite-difference time-domain (FDTD) method is developed, which does not require a partial solution of a global eigenvalue problem. In this method, a patch-based single-grid representation of the FDTD algorithm is developed to facilitate both theoretical analysis and efficient computation. This representation results in a natural decomposition of the curl–curl operator into a series of rank-1 matrices, each of which corresponds to one patch in a single grid. The relationship is then theoretically analyzed between the fine patches and unstable modes, based on which an accurate and fast algorithm is developed to find unstable modes from fine patches with a bounded error. These unstable modes are then upfront eradicated from the numerical system before performing an explicit time marching. The resultant simulation is absolutely stable for the given time step irrespective of how large it is, the accuracy of which is also ensured. In addition, both lossless and general lossy problems are addressed in the proposed method. The advantages of the proposed method are demonstrated over the conventional FDTD and the state-of-the-art explicit and unconditionally stable FDTD methods by numerical experiments.**

***Index Terms*— Explicit methods, fast methods, finite-difference time-domain (FDTD) method, stability, unconditionally stable methods.**

I. Introduction

THE finite-difference time-domain (FDTD) method is one of the most popular time-domain methods for electromagnetic analysis. This is mainly because of its simplicity and optimal computational complexity at each time step. However, the time step of a conventional FDTD [1], [2] is restricted by space step for stability, which is known as the Courant–Friedrich–Levy condition. Such a choice of time step is also the time step required by accuracy, if the space step can be determined solely from the accuracy perspective for capturing the working wavelength. However, when there are fine features relative to the working wavelength in the problem being simulated, the smallest space step can be much smaller than that determined by accuracy. Hence, the resultant time step for ensuring stability can be much smaller than that required by accuracy. As a consequence, a large number of time steps must be simulated to finish one simulation, which is time consuming.

Manuscript received October 12, 2016; revised December 23, 2016 and February 18, 2017; accepted February 25, 2017. Date of publication April 12, 2017; date of current version August 4, 2017. This work was supported in part by the National Science Foundation (NSF) under Award 1619062 and in part by the Defense Advanced Research Projects Agency (DARPA) under Award HR0011-14-1-0057.

The authors are with the School of Electrical and Computer Engineering, Purdue University, West Lafayette, IN 47907 USA (e-mail: djiao@purdue.edu).

Color versions of one or more of the figures in this paper are available online at http://ieeexplore.ieee.org.

Digital Object Identifier 10.1109/TMTT.2017.2686862

To overcome the aforementioned barrier, researchers have developed implicit unconditionally stable FDTD methods, such as the alternating-direction implicit method [3], [4], the Crank–Nicolson (CN) method [5], the CN-based split step scheme [6], the locally 1-D FDTD [7], [8], the pseudospectral time-domain method [9], the Laguerre FDTD [10], [11], the associated Hermite type FDTD [12], a series of fundamental schemes [13], and many others, but the advantage of the conventional FDTD is sacrificed in avoiding a matrix solution. Research has also been pursued [14]–[18] to address the time step problem in the original explicit time-domain methods. In [17] and [18], the source of instability in FDTD is identified to be the unstable eigenmodes whose eigenvalues are larger than what can be accurately simulated by a given time step. The unstable modes are subsequently deducted from the underlying numerical system in [17] and [18] before performing an explicit time marching. As a result, an explicit FDTD can also be made unconditionally stable. However, to find the unstable modes, [17] and [18] require a partial solution of a global eigenvalue problem. The resulting computational cost may still be high when the matrix size and/or the number of unstable modes are large.

Since the largest eigenvalue of a discretized curl–curl operator is inversely proportional to the smallest space step, the unstable modes exist indeed because of fine space discretizations relative to working wavelengths. It may not be necessary to perform a global eigenvalue solution to find the unstable modes. Along this line of thought, in this paper, we first represent the FDTD method into a *patch-based single-grid* format, in contrast to a conventional matrix representation that can be viewed as an *edge-based dual-grid* one. This new representation allows us to use patches in a single grid to formulate the FDTD, regardless of whether the grid is 2-D or 3-D. For each patch, one only needs to generate a column vector of four nonzero entries, and a row vector that is the transpose of the column vector in a uniform grid. The resultant rank-1 matrix is positive semidefinite, whose eigenvalue can also be found analytically, which we show to be inversely proportional to the patch area. This new representation helps us readily identify a theoretical and quantitative relationship between the fine patches and the largest eigenmodes of the discretized cur–curl operator. We thus prove that once there exists a difference between the time step required by stability and the time step determined by accuracy, i.e., a difference between the fine-patch size and the regular-patch size, the largest eigenmodes of the original system matrix can be extracted from fine patches with a bounded error. The larger the contrast ratio between the two time steps (or space steps), the more accurate the eigenmodes extracted in this way. This

finding can also be utilized by other research requiring finding the largest eigenmodes. Based on this theoretical finding, we propose an efficient algorithm to find the unstable modes directly from the fine patches. We then deduct these unstable modes from the numerical system of the FDTD. As a result, an explicit time marching can be performed with unconditional stability and fast.

The preliminary result of this paper has been reported in [19]. In this paper, we complete the theory behind the proposed work, which is not made clear in [19]. We also provide a detailed description of how to reformulate the FDTD method into a patch-based single-grid format, which is not given in [19]. In addition, a significant amount of work is devoted to extend the proposed method to analyze general lossy problems where both lossy dielectrics and conductors can coexist. In such a scenario, the unstable modes are much more difficult to be obtained efficiently and accurately, since the underlying eigenvalue problem is quadratic. Extensive numerical experiments are also carried out to simulate both lossless and lossy problems.

This paper is organized as follows. In Section II, we present a new way of representing the FDTD method, i.e., a patch-based single-grid representation. In Section III, we describe the proposed method for analyzing general lossless problems, where we provide a detailed theoretical analysis, elaborate step-by-step the proposed method, explain how it works, and analyze its computational efficiency. In Section IV, we develop an algorithm for analyzing general lossy problems. In Section V, a number of numerical examples are presented to demonstrate the accuracy and efficiency of the proposed new method in comparison with the original FDTD and the state-of-the-art explicit FDTD methods that are unconditionally stable. In Section VI, we summarize our findings.

II. Patch-Based Single-Grid Representation of the FDTD and Its Implication

To facilitate the development of the proposed method, we first present a new way of representing the FDTD. In the original FDTD formulation, each difference equation is written for obtaining one field unknown, either primary field unknown or dual field one, and each of these field unknowns is defined along the edge of a primary or a dual grid. Such a matrix-less formulation has also been compactly written into a matrix-based form. We can view the original FDTD formulation, either its matrix-less formulation or its matrix-based one, an *edge-based dual-grid* formulation, since each edge in the primary and dual grid is associated with one field unknown. The new representation presented in this section is a patch-based single-grid one. We use only one grid. In this grid no matter it is a 2-D or 3-D grid, we loop over all the rectangular patches present in the grid. For each patch, we formulate a column vector and a row vector, whose product is a rank-1 matrix. The row vector describes how the **E** (**H**) unknowns along the contour of the patch produce the normal **H** (**E**) field at the patch center. The column vector describes how the normal **H** (**E**) field at the patch center is used to obtain the **E** (**H**) unknowns. The two are transpose of each other in a uniform grid, but can be very different in a nonuniform grid or a grid with subgrids. With the two vectors generated for each patch, we can march on in time to find the electric and magnetic field solutions. In the following presentation of the proposed formulation, we place the normal **H** at each patch center and **E** along the edges of the grid. But the two can also be reversed.

Consider a single 2-D or 3-D grid. Denote the total number of **E** and **H** unknowns by N_e and N_h respectively. For each patch in the grid, we obtain the normal magnetic field at the patch center, h_i, as follows:

$$\left[-\frac{1}{L_i}, \frac{1}{L_i}, \frac{1}{W_i}, -\frac{1}{W_i}\right][e] = -\mu_i \frac{\partial h_i}{\partial t} \tag{1}$$

where subscript i denotes the patch index, which is also the **H** unknown index. The L_i and W_i are, respectively, the two side lengths of patch i, and μ_i is the permeability at the patch center. Defining a global unknown vector $\{e\}$ containing all electric field unknowns, (1) can be rewritten as

$$\mathbf{S}_e^{(i)}{}_{1\times N_e}\{e\} = -\mu_i \frac{\partial h_i}{\partial t} \tag{2}$$

where $\mathbf{S}_e^{(i)}$ is a row vector of length N_e, with the superscript denoting the patch index. This row vector has only four nonzero entries shown in (1), whose column indexes are the indexes of the four local electric field unknowns in global vector $\{e\}$.

In the original FDTD formulation, Ampere's law is discretized on a grid dual to the grid used for discretizing Faraday's law, resulting in

$$(\mathbf{S}_h)_{N_e\times N_h}\{h\} = \mathbf{D}_\epsilon \frac{\partial\{e\}}{\partial t} + \{j\} \tag{3}$$

where $\{h\}$ contains all of the h unknowns, $\mathbf{D}_\epsilon$ is a diagonal matrix of permittivity, and $\{j\}$ denotes a current source vector. The above can be rewritten as follows:

$$\mathbf{S}_h^{(1)}h_1 + \mathbf{S}_h^{(2)}h_2 + \cdots + \mathbf{S}_h^{(N_h)}h_{N_h} = \mathbf{D}_\epsilon \frac{\partial\{e\}}{\partial t} + \{j\} \tag{4}$$

where $\mathbf{S}_h^{(i)}$ denotes the ith column of $\mathbf{S}_h$, and the $\mathbf{S}_h\{h\}$ in (3) is realized as the sum of weighted columns, instead of a row-based computation that one is more used to. Each row of (3) represents a curl of **H** operation producing an electric field unknown, but each column does not. However, by doing so, (4) allows us to discretize Ampere's law in the original grid and on the same patch producing h_i. Each column vector $\mathbf{S}_h^{(i)}$ has only nonzero entries at the rows corresponding to the **E** unknowns generated from h_i. In a uniform grid, $\mathbf{S}_h^{(i)}$ has only four nonzero entries, and it is simply

$$\left(\mathbf{S}_h^{(i)}\right)_{N_e\times 1} = \mathbf{S}_e^{(i)T}. \tag{5}$$

In a nonuniform grid, the $\mathbf{S}_e^{(i)}$ stays the same since h_i is still centered by **E** unknowns along the patch contour; the $\mathbf{S}_h^{(i)}$ can be altered for a better accuracy. In our implementation, we observe that a length or width averaged between adjacent patches yields a much better accuracy than its nonaveraged counterpart. Hence, the L_i and W_i in $\mathbf{S}_h^{(i)}$ are changed to the

average ones between patch i and its adjacent patch that shares the same $\mathbf{E}$ unknown. Note that each row of $\mathbf{S}_h^{(i)}$ corresponds to one electric field unknown. So for an arbitrary jth row of $\mathbf{S}_h^{(i)}$, the other patch, which shares the corresponding e_j-unknown with patch i, is known.

Now, if we take a time derivative of (4), and substitute (2) into it, we obtain

$$\mathbf{D}_\epsilon \frac{\partial^2\{e\}}{\partial t^2} + \mathbf{C}\{e\} = -\frac{\partial\{j\}}{\partial t} \tag{6}$$

where

$$\mathbf{C} = \sum_{i=1}^{N_h} {\mu_i}^{-1} \left(\mathbf{S}_h^{(i)}\right)_{N_e\times 1} \left(\mathbf{S}_e^{(i)}\right)_{1\times N_e} \tag{7}$$

which is clearly the sum of a rank-1 matrix obtained from each patch.

After column vector $\mathbf{S}_h^{(i)}$ and row vector $\mathbf{S}_e^{(i)}$ are obtained for each patch, we can use them to perform a leap-frog time marching based on (2) and (4). We can also directly solve (6) as a second-order differential equation in time using a central-difference scheme. The two can be proved to be equivalent to each other.

Since the rank-1 matrix has a form of $[a][b]^T$, where $[a]$ is a column vector and $[b]^T$ is a row vector, its eigenvalue can be found analytically as the following. Basically, by observing the following eigenvalue problem of $[a][b]^T$, where λ denotes an eigenvalue, and w is the eigenvector:

$$[a][b]^T w = \lambda w \tag{8}$$

we can immediately identify its eigenvalue solution as

$$\lambda = [b]^T[a] \tag{9}$$

$$w = [a]. \tag{10}$$

Since a rank-1 matrix has only one nonzero eigenvalue, if $\lambda = [b]^T[a]$ is greater than 0, then the matrix must be positive semidefinite as the rest eigenvalues are zero. Now consider the rank-1 matrix of an arbitrary patch i in an FDTD grid

$$\mathbf{S}_i = \left(\mathbf{S}_h^{(i)}\right)_{N_e\times 1} \left(\mathbf{S}_e^{(i)}\right)_{1\times N_e}. \tag{11}$$

From (1), (5), and (9), it can be readily seen that $\mathbf{S}_i$'s eigenvalue is

$$\lambda_{\text{patch(i)}} = \frac{2}{{L_i}^2} + \frac{2}{{W_i}^2}. \tag{12}$$

For a square patch, it is simply $4/\Delta_i$, where Δ_i is the area of patch i. This eigenvalue is also the 2-norm of the rank-1 matrix, which is also the 2-norm of column vector $\mathbf{S}_h^{(i)}$ multiplied by that of row vector $\mathbf{S}_e^{(i)}$. Obviously, the contribution of every patch in an FDTD system matrix is positive semidefinite. Thus, the sum of them is also positive semidefinite. Furthermore, the smaller the patch, the larger the eigenvalue of its rank-1 matrix.

From (7) and the analysis of each rank-1 matrix, it becomes possible to find the largest k eigenvectors of the FDTD system matrix from its k columns and k rows having the largest norm. These columns and rows correspond to exactly those contributed by fine patches, as analyzed in the above. Let the sequence of $\mathbf{S}_h^{(1)}, \mathbf{S}_h^{(2)}, \ldots$ be in a descending order of vector norm, with $\mathbf{S}_h^{(1)}$'s norm being the largest and $\mathbf{S}_h^{(k+1)}$'s norm ϵ_a times smaller than $\mathbf{S}_h^{(1)}$'s norm. Since $\mathbf{S}_h^{(i)}$'s 2-norm is

$$\left\|\mathbf{S}_h^{(i)}\right\|_2 = \sqrt{\frac{2}{{L_i}^2} + \frac{2}{{W_i}^2}} \tag{13}$$

this also means that the area of patch k is about ϵ_a^2 times larger than that of patch 1. $\mathbf{C}$ can then be well approximated as

$$\tilde{\mathbf{C}} = \sum_{i=1}^{k} {\mu_i}^{-1} \mathbf{S}_h^{(i)} \mathbf{S}_e^{(i)} \tag{14}$$

with the error of $||\mathbf{C} - \tilde{\mathbf{C}}||/||\mathbf{C}||$ bounded by $O(\epsilon_a^2)$. Hence, $\tilde{\mathbf{C}}$ can be sufficient for finding $m \le k$ largest eigenvalues and their corresponding eigenvectors with good accuracy, although it cannot be used to find all eigenpairs. This also indicates that the field distribution of largest eigenmodes is actually localized in fine patches. The above analysis can still be conceptual. In the following section, we will provide a detailed study.

III. Proposed Method for Lossless Problems

A. Theoretical Analysis

As shown in [17], [18], and [20], the time step for a stable FDTD simulation, Δt_s, is required to satisfy the following criterion:

$$\Delta t_s \le \frac{2}{\sqrt{\rho(\mathbf{S})}} \tag{15}$$

where $\rho(\mathbf{S})$ denotes the spectral radius of $\mathbf{S} = \mathbf{D}_{(1/\epsilon)}\mathbf{C}$, which is the largest eigenvalue of $\mathbf{S}$. Using the eigenvalue shown in (12), dividing it by ϵ and μ, we can obtain the eigenvalue of $\mathbf{S}$ for a single patch i. This is clearly $4c^2/\Delta_i$ for a square patch, where c is the speed of light. Based on (15), we obtain $\Delta t_s \le \sqrt{\Delta_i}/c$. The largest eigenvalue of $\mathbf{S}$ is bounded by its norm. Because of a factorized form shown in (14), the $\mathbf{S}$'s norm can be readily found as no greater than the largest $c^2||\mathbf{S}_h^{(i)}|| \cdot ||\mathbf{S}_e^{(i)}|| = c^2||\mathbf{S}_h^{(i)}||^2$, and hence the largest $4c^2/\Delta_i$ as can be seen from (13). Thus, $\Delta t_s \le \sqrt{\Delta_{\min}}/c$, where $\Delta_{\min}$ is the smallest patch area. Hence, using the proposed new representation of the FDTD, we can also readily see that (15) dictates that the maximum time step permitted by stability is proportional to the smallest space step.

In [17] and [18], the eigenvectors of $\mathbf{S}$ corresponding to the largest eigenvalues, which are beyond the stability criterion, are identified as the root cause of instability. The Arnoldi algorithm is then employed to find these unstable eigenvectors. For a sparse matrix of size N_e, finding its largest k eigenpairs may take many more than k Arnoldi steps, with the computational complexity being $O(k'^2N)$, where $k' > k$. When N is large, the computational overhead for obtaining a complete set of unstable modes in [18] could still be too high to tolerate. In this section, we identify a relationship between the unstable modes and the fine patches present in the space discretization, from which a global eigenvalue problem can be avoided.

Given a time step Δt, $\mathbf{S}$ can be partitioned into two components

$$\mathbf{S} = \mathbf{S}_f + \mathbf{S}_c \tag{16}$$

where $\mathbf{S}_f$ consists of all fine patches, the rank-1 matrix of which has an eigenvalue shown in (12) larger than that permitted by the given time step, and $\mathbf{S}_c$ is composed of the rest. Consider an eigenvector, $\mathbf{F}_{hi}$, of $\mathbf{S}_f$. It satisfies

$$\mathbf{S}_f \mathbf{F}_{hi} = \lambda_i \mathbf{F}_{hi}. \tag{17}$$

Next, we prove that it also satisfies the following with a bounded error ϵ_{acc}:

$$\mathbf{S}\mathbf{F}_{hi} \overset{\epsilon_{\text{acc}}}{=} \lambda_i \mathbf{F}_{hi} \tag{18}$$

and thus the eigenvectors obtained from the fine patches are also the eigenvectors of the entire problem domain with ϵ_{acc} accuracy.

Proof: To prove (18), we evaluate the following:

$$\epsilon_{\text{acc}} = \frac{\|\mathbf{S}\mathbf{F}_{hi} - \lambda_i \mathbf{F}_{hi}\|}{\|\mathbf{S}\mathbf{F}_{hi}\|}. \tag{19}$$

Since $\mathbf{S}\mathbf{F}_{hi} = (\mathbf{S}_f + \mathbf{S}_c)\mathbf{F}_{hi}$, and $\mathbf{F}_{hi}$ satisfies (17), (19) can be rewritten as

$$\epsilon_{\text{acc}} = \frac{\|\mathbf{S}_c \mathbf{F}_{hi}\|}{\|\mathbf{S}_c \mathbf{F}_{hi} + \lambda_i \mathbf{F}_{hi}\|}. \tag{20}$$

Since $\mathbf{S}_c$ is positive semidefinite, the above satisfies

$$\epsilon_{\text{acc}} \leq \frac{\|\mathbf{S}_c\| \|\mathbf{F}_{hi}\|}{\lambda_i \|\mathbf{F}_{hi}\|} = \frac{\|\mathbf{S}_c\|}{\lambda_i}. \tag{21}$$

Since $\mathbf{S}_c$ is Hermitian, its norm is also its spectral radius, i.e., the largest eigenvalue of $\mathbf{S}_c$. This number determines the maximum time step that can be used in the regular patches for a stable simulation, denoted by Δt_c. Similarly, the maximum λ_i of $\mathbf{S}_f$ determines the time step Δt_f that can be used in the fine patches for a stable simulation, which is also equal to the Δt_s in (15) for the entire computational domain. As a result, from (21), we obtain

$$\epsilon_{\text{acc}} \leq \left(\frac{\Delta t_f}{\Delta t_c}\right)^2 = \left(\frac{\Delta t_s}{\Delta t}\right)^2. \tag{22}$$

The last equality in the above holds true because the ratio of Δt_f to Δt_c is also the ratio of time step required by stability Δt_s to that determined by solution accuracy (Δt), assuming the regular-cell region is discretized based on accuracy. From (22), it is evident that once Δt_s is smaller than Δt, which is exactly the scenario when the time step issue should be solved, the unstable eigenmodes can be obtained from fine patches with a bounded error. Meanwhile, the larger the contrast ratio of regular-patch size to the fine-patch size, the better the accuracy of the unstable eigenmodes extracted from fine patches. In addition, from (21), it can be seen among the eigenvalues λ_i obtained from the fine patches, the larger the eigenvalue, the better the accuracy. Based on the above finding, we develop a fast method to achieve unconditional stability in an explicit FDTD time marching, as shown in the next section.

B. Proposed Algorithm

The proposed method includes three steps. First, we find unstable modes accurately from fine patches with controlled accuracy. Second, we upfront deduct the unstable modes from the system matrix, and perform an explicit marching on the updated system matrix with absolute stability. Finally, we add back the contribution of unstable modes if necessary.

1) Step I: Finding Unstable Modes Accurately From Fine Patches: Given any desired time step Δt, we categorize the patches in the grid into two groups. One group, denoted by $\mathbb{C}_c$, consists of the regular patches, which allow for the use of the desired time step without becoming unstable. To be specific, the single nonzero eigenvalue of the rank-1 matrix of a regular patch divided by its permittivity and permeability is no greater than $4/\Delta t^2$. The other group $\mathbb{C}_f$ includes all the fine patches and the patches immediately adjacent to the fine patches. The rank-1 matrix of each fine patch residing in a fine grid has an eigenvalue larger than that of the regular patch. The same is true for the patches immediately adjacent to the fine patches. This is because in these patches, the length parameters L_i and W_i are averaged from the fine patch and the regular patch sharing the $\mathbf{E}$-unknown, when calculating the four nonzero elements of column vector $\mathbf{S}_h^{(i)}$. As a result, the eigenvalue of the rank-1 matrix of a patch adjacent to the fine patch is also larger than that of the regular one. Clearly, $\mathbb{C}_f$ patches require a smaller Δt to ensure the stability. These patches do not have to be connected. They can be arbitrarily located in the grid. Accordingly, $\mathbf{S}$ can be split as shown in (16), where $\mathbf{S}_f$ is $\mathbf{S}$ assembled from $\mathbb{C}_f$ and $\mathbf{S}_c$ is from $\mathbb{C}_c$. To identify $\mathbf{S}_f$, the new FDTD representation presented in Section II provides a convenient and efficient approach. Based on (7), we obtain $\mathbf{S}_f$ by looping over all the fine patches. For each patch, we obtain a rank-1 matrix $\mathbf{S}_h^{(i)}\mathbf{S}_e^{(i)}$. We then sum them up to obtain

$$\mathbf{S}_f = \mathbf{D}_{\frac{1}{\epsilon}} \sum_{i=1, i\in\mathbb{C}_f}^{k} {\mu_i}^{-1} \mathbf{S}_h^{(i)}{}_{N_e\times 1} \mathbf{S}_e^{(i)}{}^T{}_{1\times N_e} \tag{23}$$

in which k is the patch number in $\mathbb{C}_f$.

Denote the $\mathbf{E}$ unknown number in $\mathbb{C}_f$ by n. This is also the edge number in $\mathbb{C}_f$. Let the $\mathbf{H}$ unknown number in $\mathbb{C}_f$ be k. This is also the patch number in $\mathbb{C}_f$. It is evident that $n < N_e$ and $k < N_h$. The column vector $\mathbf{S}_h^{(i)}$ in (23) has only four nonzero entries, whose row indexes correspond to the fine-patch electric field unknown indexes. Similarly, the row vector $\mathbf{S}_e^{(i)}$ has four nonzero elements at the columns of the fine-patch unknowns. The matrix in (23), hence, can be rewritten as a small n by n matrix

$$\mathbf{S}_f^{(f)}{}_{n\times n} = \mathbf{A}_{n\times k}\mathbf{B}_{k\times n}^T \tag{24}$$

where $\mathbf{A}$ is composed of the k columns of $\mathbf{S}_h^{(i)}$, and $\mathbf{B}^T$ has the k rows of $\mathbf{S}_e^{(i)^T}$, where the zeros corresponding to the unknowns in regular patches are removed. The permittivity is included in $\mathbf{A}$, while the permeability is included in $\mathbf{B}$. Since k is less than n, the $\mathbf{S}_f^{(f)}$ is intrinsically low rank. We then extract l unstable eigenmodes, $\mathbf{F}_{hi}$, from $\mathbf{S}_f^{(f)}$, the complexity

of doing so is only $O(l^2n)$. Here, $l < k, i$=1, 2, ..., l. Since $l < k'$ and $n \ll N_e$, this cost is much smaller than $O(k'^2N_e)$ in [18], which is the complexity of an Arnoldi-based global eigenvalue solution. Given an accuracy threshold ϵ, if the following requirement is satisfied, the $\mathbf{F}_{hi}^{(f)}$ is accurate enough to be chosen as an unstable mode:

$$\epsilon_{acc} = \frac{\|\mathbf{S}\mathbf{F}_{hi} - \lambda_i \mathbf{F}_{hi}\|}{\|\mathbf{S}\mathbf{F}_{hi}\|} < \epsilon \tag{25}$$

where $\mathbf{F}_{hi}$ is $\mathbf{F}_{hi}^{(f)}$ extended to length N_e based on the global unknown ordering. Among l eigenvectors, assume k_r of them are accurate. They are also the k_r largest eigenvalues. We then orthogonalize them as $\mathbf{V}_h$ for the use of the next step.

When calculating ϵ_{acc}, 2-norm is used in this paper. The choice of the accuracy threshold ϵ is a user-defined parameter. Since the larger the eigenvalue, the better the accuracy of the eigenmode extracted from $\mathbf{S}_f$, we compute the eigenvalues of $\mathbf{S}_f$ starting from the largest to smaller ones. For each eigenpair computed, we calculate ϵ_{acc} defined in (19) until it is greater than prescribed ϵ. The ϵ_{acc} calculated for the largest eigenpair represents the best accuracy one can achieve in the given grid, which also dictates the smallest ϵ one can choose.

2) Step II: Explicit and Unconditionally Stable Time Marching: After the unstable modes are found, before performing the explicit time marching, we directly deduct $\mathbf{V}_h$ modes from $\mathbf{S}$ as follows:

$$\mathbf{S}_l = \mathbf{S} - \mathbf{V}_h\mathbf{V}_h^H\mathbf{S} \tag{26}$$

which permits the use of the desired time step, regardless of how large it is. The explicit marching can then be carried out using the updated system matrix as

$$\{e\}^{n+1} = 2\{e\}^n - \{e\}^{n-1} - \Delta t^2\mathbf{S}_l\{e\}^n + \Delta t^2\{f\}^n. \tag{27}$$

At each time step after finding $\{e\}^{n+1}$, the following treatment is added to ensure that $\{e\}$ is free of $\mathbf{V}_h$ modes:

$$\{e\}^{n+1} = \{e\}^{n+1} - \mathbf{V}_h\mathbf{V}_h^H\{e\}^{n+1}. \tag{28}$$

In the special case where all patches are fine patches, the proposed method is equally valid. In this case, only the nullspace of $\mathbf{S}$, $\mathbf{V}_0$, is left in $(\mathbf{S} - \mathbf{V}_h\mathbf{V}_h^H\mathbf{S})$, i.e., $(\mathbf{S} - \mathbf{V}_h\mathbf{V}_h^H\mathbf{S})$=$\mathbf{V}_0\mathbf{V}_0^H\mathbf{S}$. Since the product of $\mathbf{S}$ and $\mathbf{V}_0$ is zero, the $\mathbf{S}_l$ term vanishes in (27). The $\{e\}$'s solution, which contains only nullspace modes as ensured by (28), becomes the time integration of the right-hand side performed twice. The resultant solution is correct, as shown in [18]. Note that one cannot just take (6) and vanish the $\mathbf{S}$-related term therein for obtaining a field solution of nullspace modes (also known as DC modes). If one does so, the solution would be wrong. Only the nullspace component of the field solution makes the $\mathbf{S}$-related term vanish.

3) Step III: Adding Back the Contribution of Unstable Modes if Necessary: This step is not needed when the time step is chosen based on accuracy, since the unstable modes removed are not required by accuracy as analyzed in [18]. In the case when time step chosen is larger than that required by accuracy, some eigenvectors that are important to the field solution are also removed from the numerical system, and therefore the solution computed from (27) and (28) is no longer an accurate solution of the original problem in (6) any more. In this case, the proposed algorithm allows users to add the $\mathbf{V}_h$ contribution back to guarantee accuracy. Basically, we can express the field solution $\{e\}$ of (6) as

$$\{e\} = \mathbf{V}\{y\} = \mathbf{V}_l\{y_l\} + \mathbf{V}_h\{y_h\} = \{e_l\} + \{e_h\} \tag{29}$$

where $\mathbf{V}$=[$\mathbf{V}_l$, $\mathbf{V}_h$] is orthogonal of full rank N_e. Since from (27) and (28), $\{e_l\}$ has been obtained, we need to find only $\{e_h\}$. Since $\mathbf{V}_h$ has been computed, front multiplying $\mathbf{V}_h^H$ on both sides of (6), the $\{y_h\}$ can be readily found from

$$\frac{\partial^2\{y_h\}}{\partial t^2} + \mathbf{S}_r\{y_h\} = \mathbf{V}_h^T\big(\{f\} - \mathbf{S}\{e_l\}\big) \tag{30}$$

where $\mathbf{S}_r$=$\mathbf{V}_h^H\mathbf{S}\mathbf{V}_h$, whose size k_r is the number of unstable modes. Since (30) is of small size k_r, it can be efficiently solved by the algorithm in [17], or by implicit methods.

C. How Does It Work?

Apparently, since the proposed algorithm also allows one to add the $\mathbf{V}_h$ contribution back, it seems that any orthogonal space $\mathbf{V}_h$ can be used. This is not true. To obtain a correct solution from (27) and (28), $\mathbf{V}_h$ should satisfy $\mathbf{V}_l^T\mathbf{S}\mathbf{V}_h = 0$. This can be found as follows. Since $\{e\}$ can be expanded as (29), (6) can be rewritten as

$$\frac{\partial^2\left(\mathbf{V}_l\{y_l\} + \mathbf{V}_h\{y_h\}\right)}{\partial t^2} + \mathbf{S}\left(\mathbf{V}_l\{y_l\} + \mathbf{V}_h\{y_h\}\right) = \{f\}. \tag{31}$$

By multiplying the above by $\mathbf{V}_l^H$, we can obtain the $\mathbf{V}_l$-component of $\{e\}$ by solving

$$\frac{\partial^2\{y_l\}}{\partial t^2} + \mathbf{V}_l^H\mathbf{S}\big(\mathbf{V}_l\{y_l\} + \mathbf{V}_h\{y_h\}\big) = \mathbf{V}_l^H\{f\}. \tag{32}$$

If $\mathbf{V}_l^H\mathbf{S}\mathbf{V}_h$ is not equal to zero, (32) cannot be reduced to an equation of $\{y_l\}$ only. Only when $\mathbf{V}_l^H\mathbf{S}\mathbf{V}_h = 0$, (32) can be reduced to (27), where $\{e\} = \{e_l\}$ due to (28), and $\mathbf{I} - \mathbf{V}_h\mathbf{V}_h^H = \mathbf{V}_l\mathbf{V}_l^H$.

Since (25) is satisfied, $\mathbf{F}_h$ is an accurate eigenvector of $\mathbf{S}$. With $\mathbf{V}_h$ orthogonalized from $\mathbf{F}_h$, the property of $\mathbf{V}_l^H\mathbf{S}\mathbf{V}_h = 0$ is satisfied. This is because $\mathbf{S}\mathbf{V}_h = \mathbf{S}\mathbf{F}_h\mathbf{Z} = \mathbf{F}_h\Lambda_h\mathbf{Z} = \mathbf{V}_h\mathbf{Z}^{-1}\Lambda_h\mathbf{Z}$, and $\mathbf{V}_l^H\mathbf{V}_h = 0$. Here, we use the relationship of $\mathbf{V}_h = \mathbf{F}_h\mathbf{Z}$ where $\mathbf{Z}$ is a full-rank transformation matrix, as $\mathbf{V}_h$ is orthogonalized from $\mathbf{F}_h$.

D. Computational Efficiency

In the proposed method, we avoid finding the eigensolutions of the original global system matrix $\mathbf{S}$. Instead, we work on a much smaller matrix $\mathbf{S}_f$. Therefore, compared with the approach developed in [18], the proposed method can achieve unconditional stability more efficiently without sacrificing accuracy. The complexity of finding unstable modes is reduced significantly from the original $O(k'^2N_e)$ to $O(l^2n)$ with $n \ll N_e$ and $l < k'$. This small cost is also a one-time cost, which is performed before time marching. Since the unstable modes found in this paper are frequency and time independent, once found, they can be reused for different simulations of the same physical structure. In the second step of explicit time marching, the matrix-free property of the FDTD is preserved. The time marching has a strict linear (optimal) complexity at each time step.

IV. Proposed Method For Lossy Problems

In the previous section, we focus on lossless problems. When there exist lossy dielectrics and conductors, we need to add one more term to (6) as follows:

$$\frac{\partial^2\{e\}}{\partial t^2}+\mathbf{D}\frac{\partial\{e\}}{\partial t}+\mathbf{S}\{e\}=\{f\} \tag{33}$$

where $\mathbf{D}$ is diagonal with its ith entry being σ_i/ϵ_i at the point of the ith $\mathbf{E}$ unknown. Different from a lossless problem, (33) is governed by the following quadratic eigenvalue problem:

$$(\lambda^2+\lambda\mathbf{D}+\mathbf{S})v=0. \tag{34}$$

The treatment of such a problem is different from that of a generalized eigenvalue problem. We hence use a separate section to describe our solution to general lossy problems.

A. Theoretical Analysis

The second-order differential equation (33) can be transformed to the following first-order equation in time without any approximation:

$$\frac{\partial\{\tilde{e}\}}{\partial t}-\mathbf{M}\{\tilde{e}\}=\{\tilde{f}\} \tag{35}$$

where $\{\tilde{f}\}=[0 \quad f]^T$, $\{\tilde{e}\}=[e \quad \dot{e}]^T$, in which $\dot{e}$ denotes the first-order time derivative of e, and matrix $\mathbf{M}$ is

$$\mathbf{M}=\begin{bmatrix}0 & \mathbf{I}\\ -\mathbf{S} & -\mathbf{D}\end{bmatrix} \tag{36}$$

where $\mathbf{I}$ is an identity matrix. Obviously, $\{\tilde{e}\}$'s upper part is the original field solution of (33).

The solution of (35) is governed by the following generalized eigenvalue problem:

$$\mathbf{M}x=\lambda x. \tag{37}$$

This problem is also equivalent to (34) using the relationship of $x=[v \quad \lambda v]^T$. Since $\mathbf{I}$ is positive definite, $\mathbf{D}$ is positive semidefinite, and $\mathbf{S}$ is positive semidefinite, the eigenvalues of (37) either are nonpositive real or come as complex conjugate pairs whose real part is less than zero. Similar to lossless problems, to achieve unconditional stability, we also need to remove the unstable modes from the system matrix, now $\mathbf{M}$. These modes are analyzed in [21]. They have eigenvalues whose magnitude satisfies

$$|\lambda|>\frac{2}{\Delta t}. \tag{38}$$

Again, given a desired time step, the unstable modes have the largest eigenvalues in magnitude. Compared with lossless problems, now it is even more computationally expensive to find these unstable modes since $\mathbf{M}$ is double sized and can be highly ill-conditioned when conductor loss is involved. Therefore, similar to what we do for lossless problems, we propose to find the unstable modes efficiently from the fine patches only.

B. Proposed Method

When dealing with lossless problems, all the patches in the computational domain are divided into two groups, $\mathbb{C}_f$ and $\mathbb{C}_c$, based on the time step permitted by their grid size. For lossy problems, we incorporate into $\mathbb{C}_f$ not only the fine patches and their immediately adjacent patches, but also all the patches filled with conductive metals. This is because the conductive materials contribute eigenvalues as large as conductivity divided by permittivity. To explain, the lowest eigenmode of (34) satisfies $\mathbf{S}v=0$, which is a gradient field. For this field, in addition to zero eigenvalues, there is a set of eigenvalues whose magnitude is approximately $||\mathbf{D}||$, which is σ over permittivity. Hence, the conductive region is included since unstable modes correspond to the largest eigenvalues.

After $\mathbb{C}_f$ is identified, we can form a matrix $\mathbf{M}_f$ as follows:

$$\mathbf{M}_f=\begin{bmatrix}0 & \mathbf{I}\\ -\mathbf{S}_f & -\mathbf{D}_f\end{bmatrix} \tag{39}$$

where $\mathbf{S}_f$ can be found in the same way as (24) and $\mathbf{D}_f$ is obtained by selecting the diagonal entries of $\mathbf{D}$ corresponding to the field unknowns in $\mathbb{C}_f$. As a result, $\mathbf{M}_f$ is a $2n\times 2n$ matrix, which is much smaller than the original size of $\mathbf{M}$. We then extract the largest eigenpairs of $\mathbf{M}_f$ using the Arnoldi method. Similarly, an accuracy check similar to (25) (with $\mathbf{S}$ replaced by $\mathbf{M}$) is performed to select accurate unstable modes obtained from $\mathbf{M}_f$. Let k_r be the unstable eigenmodes obtained from $\mathbf{M}_f$, the complexity of finding them is simply $O\left(k_r^2 n\right)$. We then orthogonalize the unstable modes obtained, and augment them with zeros based on the global unknown indexes to build $\mathbf{V}_h$.

Using $\mathbf{V}_h$, we upfront deduct their contributions from the system matrix before time marching as follows:

$$\mathbf{M}_l=\mathbf{M}-\mathbf{V}_h\mathbf{V}_h^H\mathbf{M}. \tag{40}$$

We then perform a time marching of (35) using the updated system matrix $\mathbf{M}_l$ as follows:

$$\frac{\partial\{\tilde{e}\}}{\partial t}-\mathbf{M}_l\{\tilde{e}\}=\{\tilde{f}\}. \tag{41}$$

If we perform a forward-difference-based time marching on (41), the resultant update equation is definitely explicit. However, the stability requirement on the time step is $\Delta t\le -2Re(\lambda)/|\lambda|^2$ where λ is the eigenvalue of $\mathbf{M}_l$. This results in a time step smaller than $\Delta t\le 2/|\lambda|$, which is the time step required by a central-difference discretization of the original second-order (33), for stably simulating the same set of λ. To solve this problem, we propose to perform a backward difference as shown in the following:

$$(\mathbf{I}-\Delta t\mathbf{M}_l)\{\tilde{e}\}^{n+1}=\{\tilde{e}\}^n+\Delta t\{\tilde{f}\}^{n+1}. \tag{42}$$

A z-transform of the above results in $z=1/(1-\lambda\Delta t)$. Since λ of $\mathbf{M}_l$ has a nonpositive real part, the stability of (42) is ensured for any large time step. Using the accuracy determined time step Δt, and with the corresponding unstable modes removed, all the eigenvalues of $\mathbf{M}_l$ satisfy

$$|\lambda|\le\frac{1}{\Delta t}. \tag{43}$$

Hence, the inversion of the left-hand matrix of (42) can be replaced by a series expansion with a small number of terms. Thus, (42) can be explicitly marched on in time as follows:

$$\{\tilde{e}\}^{n+1} \approx (\mathbf{I}+\Delta t\mathbf{M}_l+(\Delta t\mathbf{M}_l)^2+\cdots+(\Delta t\mathbf{M}_l)^p)\{\tilde{y}\} \quad (44)$$

where $\{\tilde{y}\}$ represents the right-hand-side term in (42). In the above, there is no need to compute the matrix–matrix product. Instead, (44) is a summation of p vectors, and every vector can be obtained by multiplying the previous vector by $\mathbf{M}_l$. Hence, the computational cost of (44) is simply p matrix–vector multiplications, and $p < 10$.

To make sure that the solution is free of unstable modes, we need to add the following treatment after (44) at each time instant:

$$\{\tilde{e}\}^{n+1} = \{\tilde{e}\}^{n+1} - \mathbf{V}_h\mathbf{V}_h^H\{\tilde{e}\}^{n+1}. \quad (45)$$

C. Matrix Scaling

When conductor loss and/or multiscale structures are involved, **I**, **D**, and **S** can be orders of magnitude different in their matrix norm. The solution of the generalized eigenvalue problem (37) may have a poor accuracy. To improve the accuracy of finding unstable modes from $\mathbf{M}_f$, we adopt an optimal scaling technique introduced in [22]. Based on this technique, the **I** and **S** in (36) are scaled to

$$\tilde{\mathbf{I}} = \alpha\mathbf{I} \quad \tilde{\mathbf{S}} = \mathbf{S}/\alpha \quad (46)$$

where

$$\alpha = \sqrt{\|\mathbf{S}\|_2}. \quad (47)$$

Consequently, the first-order double-sized system (35) is updated as follows:

$$\frac{\partial\{\tilde{e}'\}}{\partial t} - \tilde{\mathbf{M}}\{\tilde{e}'\} = \{\tilde{f}'\} \quad (48)$$

where $\{\tilde{e}'\} = [e \quad \dot{e}/\alpha]^T$, $\{\tilde{f}'\} = [0 \quad f/\alpha]^T$, and $\tilde{\mathbf{M}}$ is

$$\tilde{\mathbf{M}} = \begin{bmatrix} 0 & \tilde{\mathbf{I}} \\ -\tilde{\mathbf{S}} & -\mathbf{D} \end{bmatrix}. \quad (49)$$

The $\mathbf{M}_f$ formulated for fine patches is also scaled accordingly. As can be seen in (48), the upper half of the solution vector $\{\tilde{e}'\}$ is the same as that of (35).

V. Numerical Results

In this section, we simulate a number of 2-D and 3-D examples involving inhomogeneous materials and lossy conductors to demonstrate the validity and efficiency of the proposed fast unconditionally stable FDTD method. Both small and largest contrast ratios are considered between fine and regular patches. A nonuniform grid is used to discretize fine features. As shown in [23] and [24], a naive nonuniform grid can produce errors and numerical artifacts in the field solution of the FDTD simulation. A good nonuniform grid should minimize the solution error. In the proposed implementation, the length parameters used in the column vector of each patch are averaged from adjacent patches. They have shown to produce a better accuracy, compared with nonaveraged ones. In addition, the proposed method can also be applied to subgridding. Its validity is independent of how the rank-1 matrix for each fine patch is generated. As shown in Section II, using the proposed new way of representing FDTD, the difference between a uniform grid, a nonuniform grid, and a grid with subgrids is simply the difference in the column vector and the row vector generated from each patch. The proposed method remains the same regardless of the content of the column and the row vector generated from each patch.

A. Validation of the Proposed Method

First, we did a detailed case study to validate the proposed method from a variety of aspects. A wave propagation as well as a cavity problem in a 2-D rectangular region is considered. The grid is shown in Fig. 1(a), where fine patches are introduced to examine the unconditional stability of the proposed method. Along the y-axis, the cell size is uniform of 0.1 m width. Along the x-axis, we define $Contrast\ Ratio = \Delta x_c/\Delta x_f$ where $\Delta x_c = 0.1$ m, and Δx_f is controlled by $Contrast\ Ratio$. There are three fine patches along the x-axis whose cell size is Δx_f. The total number of **E** unknowns is 258. The incident electric field is $\mathbf{E}^{\text{inc}} = \hat{y}2(t - t_0 - x/c)e^{-(t-t_0-x/c)^2/\tau^2}$ with $c = 3\times10^8$ m/s, $\tau = 2\times10^{-8}$ s, and $t_0 = 4\tau$. The regular grid size, $\Delta x_c = 0.1$ m, satisfies accuracy for capturing frequencies present in the input spectrum, which is about $1/20$ of the smallest wavelength. The computational domain is terminated by an exact absorbing boundary condition, which is the known total field. This is because for any problem, the total fields on the boundary serve as an exact absorbing boundary condition to truncate a computational domain. For most of the problems, such fields are unknown. However, in a free-space problem studied in this example, the total field is known since it is equal to the incident field.

When choosing $Contrast\ Ratio = 100$, Δx_f=0.001 m, which is two orders of magnitude smaller than that required by accuracy. Hence, there is a two orders of magnitude difference between the time step required by accuracy and that by stability. The conventional FDTD method must use a time step no greater than 3.84×10^{-12} s to perform a stable simulation. In contrast, the proposed method is able to use a time step of 2.42×10^{-10} s solely determined by accuracy to carry out the simulation. The fine patches and their adjacent patches are identified, which are marked in red in Fig. 1(a). They involve 50 internal **E** unknowns. Therefore, the size of $\mathbf{S}_f$ is 50 by 50, from which 15 unstable eigenmodes are found accurately for a prescribed accuracy of $\epsilon = 10^{-6}$. The ϵ_{acc} for the 16th eigenmode in (25) is 0.1036. Hence, the 16th eigenmode and thereafter are not selected since their accuracy does not meet the required accuracy. The 15 unstable modes are then deducted from the system matrix, permitting a two-orders-of-magnitude larger time step. In Fig. 1(b), the electric fields at two observation points marked by blue cross in Fig. 1(a) are plotted as a function of time. Obviously, they show excellent agreement with reference analytical solutions.

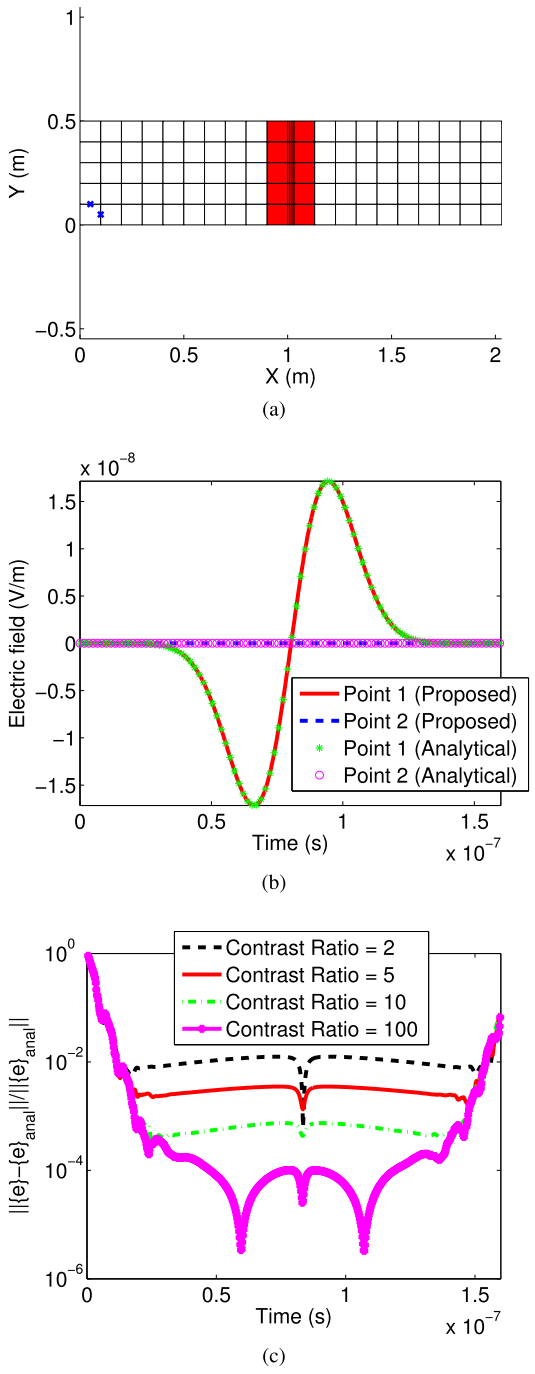

Fig. 1. Simulation of a wave propagation in a 2-D grid. (a) Space discretization. (b) Simulated electric fields at two observation points when *Contrast Ratio* = 100. (c) *Entire* solution error versus time with different *Contrast Ratio* from 2, 5, and 10 to 100.

In this example, we have also numerically examined whether the eigenmodes extracted from the fine patches are accurate approximations of the eigenmodes of the entire problem. In Table I, we list the eigenvalues of the 15 unstable modes and also the 16th one we extract from $\mathbf{S}_f$ with *Contrast Ratio* = 100. It is clear to see that the largest 15 eigenvalues are at least two orders of magnitude larger than the 16th one. Once they are removed, a much larger time step can be used for a stable simulation. In Table II, we list the accuracy of each unstable eigenmode with respect

TABLE I

LARGEST 16 EIGENVALUES OBTAINED FROM $\mathbf{S}_f$ WHEN *Contrast Ratio* = 100

λ_1	2.70260697E+25
λ_2	2.70251709E+25
λ_3	2.70240599E+25
λ_4	2.70228179E+25
λ_5	2.70231612E+25
λ_6	9.16900389E+24
λ_7	9.16810512E+24
λ_8	9.16699417E+24
λ_9	9.16575210E+24
λ_{10}	9.166095405E+24
λ_{11}	1.23429421E+22
λ_{12}	1.22530647E+22
λ_{13}	1.21419701E+22
λ_{14}	1.20177625E+22
λ_{15}	1.20520926E+22
λ_{16}	5.89575274E+19

to different *Contrast Ratios* from 2, 5, and 10 to 100, by calculating the relative error shown in (19). Obviously, for all these contrast ratios, the eigenmodes extracted from fine patches are shown to be accurate eigenmodes of the entire $\mathbf{S}$. Furthermore, the larger the contrast ratio of fine patches to the coarse ones, the better the accuracy of the eigenmodes found from fine patches. Moreover, the eigenmodes whose eigenvalues are larger are more accurate. All of these have verified our theoretical analysis given in Section III. Note that when *Contrast Ratio* = 2, the number of unstable eigenmodes that can be accurately extracted is smaller. However, we still can obtain a set of eigenmodes accurately for such a small contrast ratio.

To examine the solution accuracy at all points in the grid, we define the entire solution error at each time instant as

$$\text{Entire Solution Error} = \frac{\|\{e\}_{N_e\times 1} - \{e\}_{\text{anal}N_e\times 1}\|}{\|\{e\}_{\text{anal}}\|_{N_e\times 1}} \quad (50)$$

where $\{e\}_{N_e\times 1}$ consists of *all* electric field unknowns generated by the proposed method and $\{e\}_{\text{anal}}$ is the analytical solution to all the unknowns. For example, considering an $\mathbf{E}$ unknown located at $\mathbf{r}_i$ with direction $\hat{t}_i$, its analytical solution for this wave propagation problem is simply $\mathbf{E}^{\text{inc}}(\mathbf{r}_i)\cdot\hat{t}_i$. Two-norm is used to calculate (50) in this paper. Meanwhile, we examine the solution accuracy as a function of *Contrast Ratio*. The entire solution error is plotted in Fig. 1(c) for four different *Contrast Ratios* 2, 5, 10, and 100, respectively. It is evident that the solution accuracy of the proposed method is satisfactory for all these contrast ratios. Furthermore, the larger the contrast ratio, the better the accuracy. In this example, we also use the conventional FDTD method with $\Delta t = 3.84\times 10^{-12}$ s to simulate the case with *Contrast Ratio* = 100, and plot the entire solution error versus time in Fig. 2. Comparing Fig. 1(c) with Fig. 2 for *Contrast Ratio* = 100, it is obvious that the proposed method can achieve the same level of accuracy as the conventional FDTD method. As for efficiency, the CPU time speedup is 1.58, 3.08, and 28.16, respectively, for contrast ratios of 5, 10, and 100. However, no speedup is observed when contrast ratio is two, because of the small time step difference and the additional overhead of the proposed method. The proposed method takes 0.0563 s including the CPU time

TABLE II
ACCURACY OF EACH UNSTABLE EIGENMODE OBTAINED FROM $\mathbf{S}_f$ WITH DIFFERENT *Contrast Ratio*

CR	$\mathbf{F}_{h1}$	$\mathbf{F}_{h2}$	$\mathbf{F}_{h3}$	$\mathbf{F}_{h4}$	$\mathbf{F}_{h5}$	$\mathbf{F}_{h6}$	$\mathbf{F}_{h7}$	$\mathbf{F}_{h8}$	$\mathbf{F}_{h9}$	$\mathbf{F}_{h10}$	$\mathbf{F}_{h11}$	$\mathbf{F}_{h12}$	$\mathbf{F}_{h13}$	$\mathbf{F}_{h14}$	$\mathbf{F}_{h15}$
2	2.9e-3	2.9e-3	2.8e-3	2.6e-3	2.5e-3	1.7e-2	1.8e-2	1.9e-2	1.9e-2	1.9e-2					
5	4.4e-5	4.1e-5	3.6e-5	3.0e-5	2.8e-5	6.0e-4	5.7e-4	5.1e-4	4.5e-4	4.2e-4	2.2e-2	2.4e-2	2.7e-2	2.8e-2	2.9e-2
10	1.6e-6	1.4e-6	1.2e-6	1.0e-6	9.6e-7	3.0e-5	2.7e-5	2.4e-5	2.0e-5	1.9e-5	6.8e-3	7.1e-3	7.4e-3	7.6e-3	7.5e-3
100	1.7e-11	1.6e-11	1.4e-11	1.1e-11	1.0e-11	4.5e-10	4.0e-10	3.5e-10	3.0e-10	2.7e-10	8.3e-5	8.2e-5	8.0e-5	7.7e-5	7.6e-5

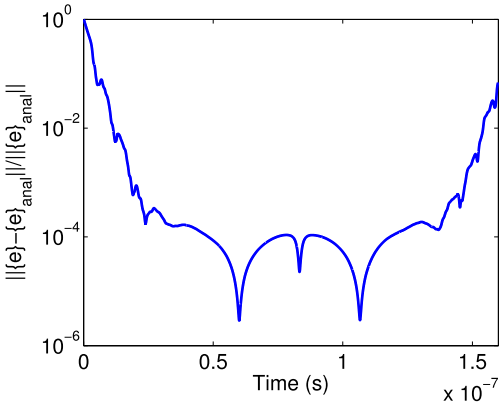

Fig. 2. Conventional FDTD for wave propagation problem: *entire* solution error versus time with $Contrast\ Ratio = 100$.

of every step from finding the unstable eigenmodes to explicit time marching, while the conventional FDTD method only requires 0.0367 s to finish the simulation. We have also studied a cavity problem using the same mesh [25], which again reveals an excellent agreement between the proposed method and the conventional FDTD.

In Fig. 3, we plot three eigenvectors of $\mathbf{S}$ whose eigenvalues are, respectively, the largest, the fifth largest, and the 15th largest eigenvalues of global $\mathbf{S}$, for a contrast ratio of 100. As can be seen from Fig. 3, the field distributions of these eigenvectors are localized in the fine patches, with the fields in the regular patches many orders of magnitude smaller. For example, for the 15th largest eigenmode whose field distribution is more spread over than the first two, its eigenmode (eigenvector) still has a field value in the immediately adjacent coarse patches being three orders of magnitude smaller than that in the fine patches. Fig. 3 further confirms that the highest eigenmodes can be accurately extracted from fine patches. Although it is plotted for contrast ratio 100, similar localizations have been observed for other smaller contrast ratio, which can also be seen from the small error of eigenvectors extracted from $\mathbf{S}_f$ listed in Table II. Numerically, such a localization is because the rapid field variation of the large-eigenvalue modes cannot be captured by a coarse discretization. This is similar to the fact that if one uses a coarse grid to extract the cavity resonance frequencies, the frequencies (eigenvalues) one can numerically identify are much smaller than the ones he can find using a fine grid. Analytically, all these eigenvalues should exist in the solution domain. However, numerically, only finer patches can capture larger eigenvalues. It should also be mentioned that removing unstable modes is not the same as removing fine features or patches, since the stable eigenmodes kept in the numerical system also capture the fine features, i.e., these modes are

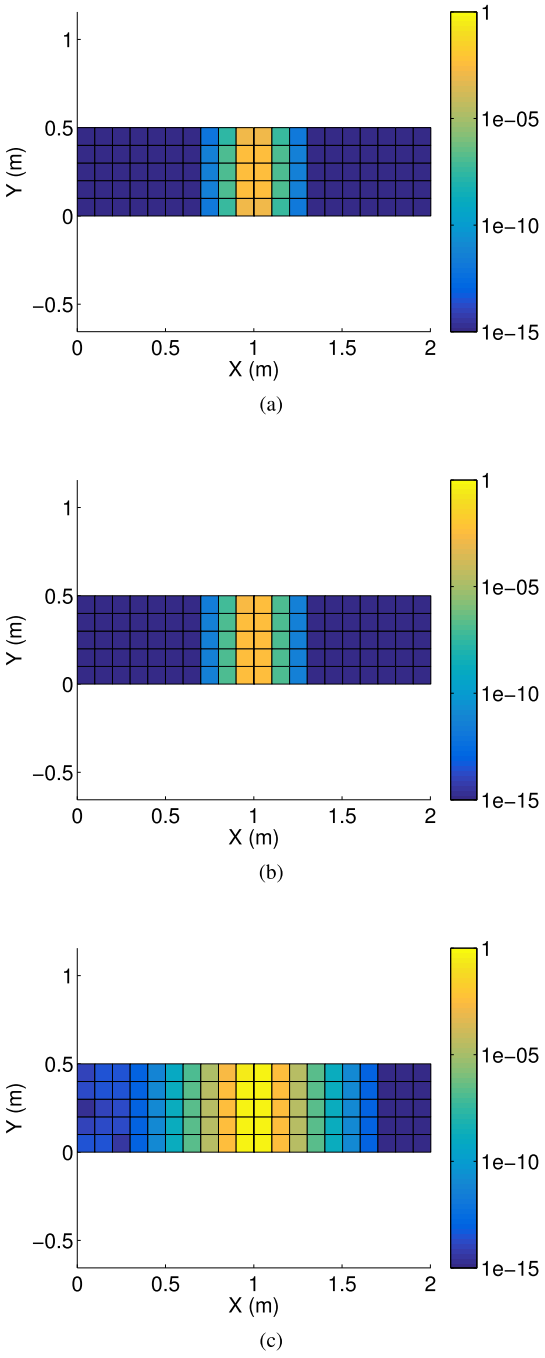

Fig. 3. Field distribution of the eigenvectors of $\mathbf{S}$ for a contrast ratio of 100 plotted in log scale. (a) Eigenvector having the largest eigenvalue. (b) Eigenvector having the fifth largest eigenvalue. (c) Eigenvector having the 15th largest eigenvalue.

different when there are fine features and when there are not. Note that each eigenmode is a source-free solution in the given problem satisfying all boundary conditions at the material

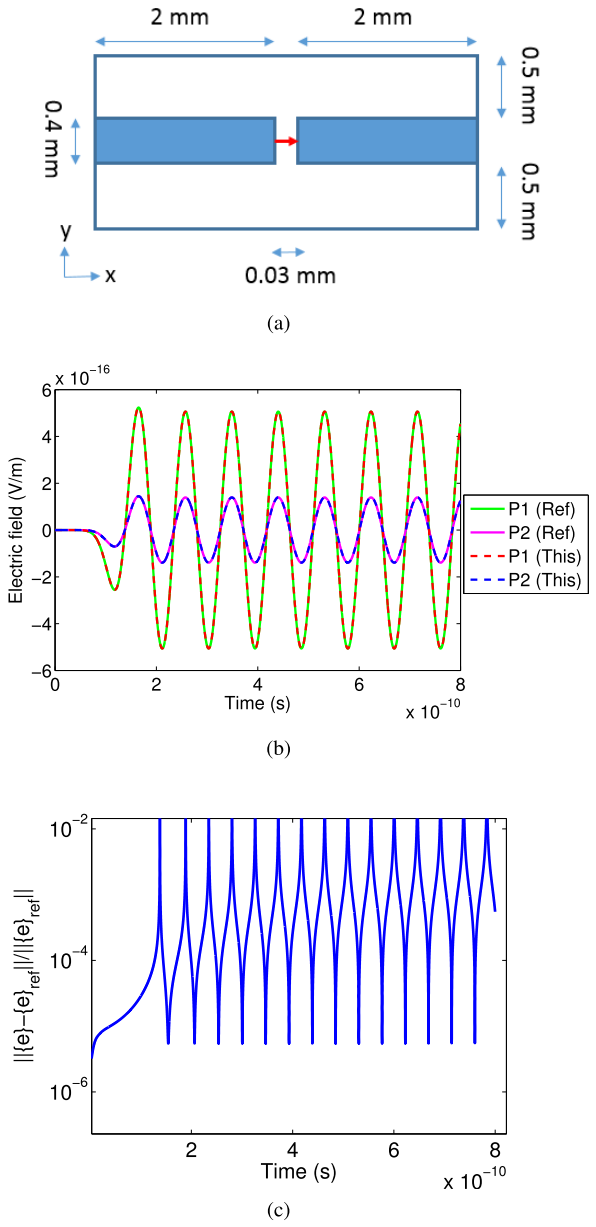

Fig. 4. Simulation of a cavity with fins. (a) Structure illustration. (b) Electric fields at two observation points. (c) *Entire* solution error as a function of time in comparison with reference solution.

interface. The eigenvalue of an eigenmode does not reflect the spatial frequency. For example, a zero-eigenvalue mode (a static field distribution) also has rapid space variations.

B. Demonstration of Accuracy and Efficiency

After an extensive validation of the proposed method, we simulate a variety of lossless and lossy examples to demonstrate the accuracy and efficiency of the proposed new method compared with the conventional FDTD and the state-of-the-art unconditionally stable explicit FDTD method like [18].

1) Conductive Fins Separated by a Narrow Gap: In this example, we simulate a 2-D PEC cavity with two conductive fins separated by a narrow gap. The details of the structure are shown in Fig. 4(a). The conductive fins are treated as perfect conductors. Between the two fins, there is a small gap discretized into three fine grids of width 0.01 mm each along the x-direction. The regular grid size is 0.1 mm along both the x- and y-directions. The discretization results in 1261 edges and 602 patches. An x-orientated current source is launched between the two fins and its waveform is $I = -\tau^2 \exp -(t - t_0/\tau)^2$, where τ=3 $\times$ 10^{-11} s and $t_0 = 4\tau$. For this example, 28 unstable modes are extracted from $\mathbf{S}_f$ with $\epsilon = 10^{-6}$. $\mathbf{S}_f$ is a square matrix of size 123 assembled from fine patches only. After unstable modes are removed from the system matrix, we can enlarge the time step from 3.7×10^{-14} to 1.59×10^{-13} s. The total CPU time required is 0.4451 s including the time for finding unstable modes. As a comparison, the explicit unconditionally stable FDTD method [18] can also increase the time step to the same value, but it takes 0.5733 s to finish the simulation. The traditional FDTD method costs 0.9536 s to finish the simulation. Therefore, the proposed method is more efficient.

To assess accuracy, the electric fields at two points located at (1.0, 0.4) and (2.0, 1.1) mm are plotted in comparison with the reference result obtained from the traditional FDTD in Fig. 4(b). It is evident that the results from the proposed method agree with the reference results very well. Meanwhile, the entire solution error (50), which includes the error at all points in the grid, is plotted versus time in Fig. 4(c). It is shown to be small across the whole time window, validating the accuracy of the proposed method.

2) 3-D Wave Propagation: A wave propagation problem is simulated in a 3-D free space. The incident field is the same as that of the first example. We also supply an exact absorbing boundary condition to all the unknowns on the boundary. Unlike the first example that has an abruptly changed grid size, a progressively changed grid size is adopted for space discretization. The space step is 0.1 m along both the y- and z-directions. There are five cells along each of the two directions. The grid along the x-direction has 13 cells, each of which is of width 0.1 m except for the three cells in the middle whose space step is 0.01, 0.001, and 0.01 m, respectively.

The time step of a conventional FDTD is less than 1.07×10^{-11} s, whereas the time step of the proposed method is 2.0×10^{-10} s chosen based on sampling accuracy. The electric fields obtained from the proposed method are plotted in Fig. 5(a) at two points, (0.51, 0.45, 0.2) and (0.57, 0.4, 0.2) m, respectively. Excellent agreement with analytical solutions can be seen. In Fig. 5(b), we plot the entire solution error, $\|\{e\} - \{e\}_{\text{anal}}\|/\|\{e\}_{\text{anal}}\|$, compared with the analytical solution, which reveals that the proposed method is accurate at all points and across the whole time window simulated. It is worth mentioning that the large errors at early and late time are expected, since the theoretical error is infinity at these times due to a zero denominator, since the field solution is zero.

In this simulation, the number of fine patches is 350. The $\mathbf{A}$ ($\mathbf{B}$) shown in (24) is of size 320 by 350. Given ϵ=10^{-2}, we obtain 120 unstable eigenmodes accurately from $\mathbf{S}_f$. It takes the proposed method 0.6470 s to finish the simulation. To simulate the same example, a conventional FDTD costs 2.1608 s. The state-of-the-art unconditionally stable explicit FDTD method in [18] spends 0.3629 s in finding the unstable modes and 1.2545 s for explicit marching. Hence, the proposed

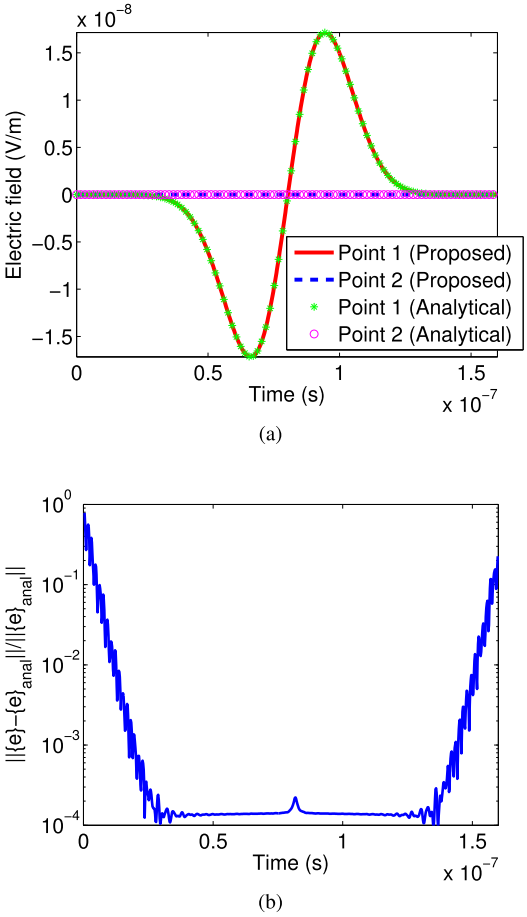

Fig. 5. Simulation of a 3-D wave propagation problem. (a) Electric fields at two observation points. (b) *Entire* solution error with respect to time.

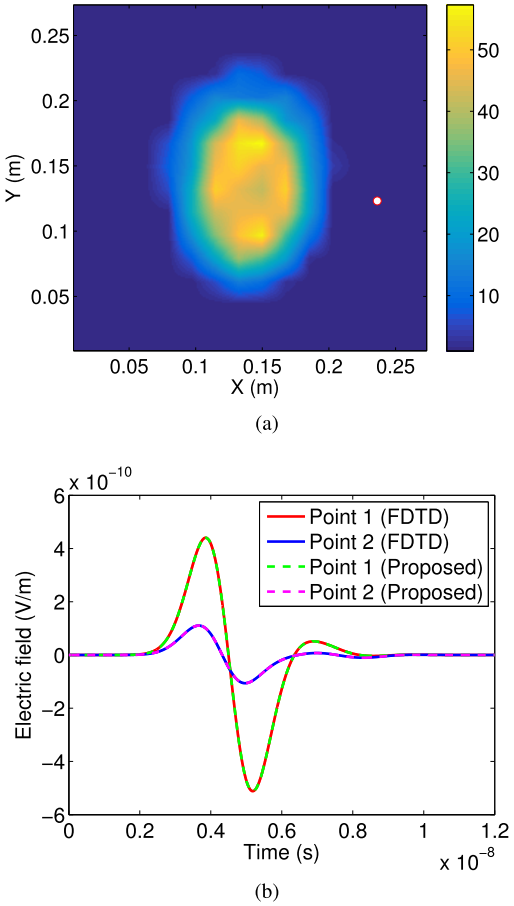

Fig. 6. Simulation of a phantom head beside a wire antenna. (a) Relative permittivity distribution in a cross section of the phantom head at z = 2.8 cm. (b) Simulated electric field at two observation points in comparison with reference FDTD solutions.

method is faster than both methods. This is because the method in [18] finds unstable modes from a global $\mathbf{S}$ matrix. In addition, the $\mathbf{V}_h$ in [18] is dense. In contrast, the $\mathbf{V}_h$ in this new method is zero in regular patches, thus speeding up the explicit time marching step as well.

3) Inhomogeneous 3-D Phantom Head Beside a Wire Antenna: Previous examples are in free space. The third example is a large-scale phantom head [26] beside a wire antenna, which involves many inhomogeneous materials. The permittivity distribution of the head at z=2.8 cm is shown in Fig. 6(a). The wire antenna is located at (24.64, 12.32, 13.44) cm as marked by the white dot in Fig.6(a), the current on which has a pulse waveform of $\mathbf{J}$=$2(t-t_0)e^{-(t-t_0)^2/\tau^2}$ with τ=1.0×10^{-9} s and t_0=4τ. The size of the phantom head is 28.16 cm × 28.16 cm × 17.92 cm. The coarse step size along the x-, y-, and z-directions is 17.6, 17.6, and 1.4 mm, respectively, which results in 109 667 unknowns. To capture the fine tissues located at the center of this head, three layers of fine grid whose lengths are 1.4 μm are added in the middle along the z-direction. As a result, the conventional FDTD method can use only a time step less than 5.39×10^{-15} s to ensure stability. In the proposed method, 768 fine patches are identified, which involve 4709 electric field unknowns and 4256 magnetic field unknowns. Given ϵ=10^{-7}, 1088 unstable eigenmodes are obtained accurately from $\mathbf{S}_f$. With the contribution of unstable eigenmodes removed, the time step is increased to 2.56×10^{-13} s. In Fig. 6(b), the electric fields at two points (12.32, 3.52, 13.44) and (12.32, 24.64, 13.44) cm are plotted in comparison with reference FDTD results. Again, very good agreement is observed. As for CPU time, the proposed method takes 84.8142 s to extract unstable eigenmodes and 2895.7305 s for explicit time marching. However, the conventional FDTD needs 29968.7009 s to finish the same simulation. Meanwhile, although the method developed in [18] can also boost the time step up to the same value as the proposed method, it requires 8268.2 s instead in CPU time. Therefore, the proposed method is not only much faster than the conventional FDTD method, it is also more efficient than [18] since the proposed method requires the fine region only instead of the entire computational domain to extract unstable eigenmodes.

4) Inhomogeneous and Lossy 3-D Microstrip Line Structure: A microstrip line illustrated in Fig. 7(a) is simulated. It has lossy conductors and inhomogeneous dielectrics. A 3-D view of the structure can be seen in Fig. 7(a), and the structure is 4 mm long along the y-direction. A current source is injected between the bottom plate and the strip. It has a pulse of $\mathbf{I}=\hat{z}2(t-t_0)e^{-(t-t_0)^2/\tau^2}$ A, where $\tau=10^{-10}$ s and $t_0=4\tau$ s. The space step is 0.4 mm in all directions, but to capture skin effects in lossy conductors, the microstrip is discretized into 0.15, 0.15, and 34.7 μm in the z-direction,

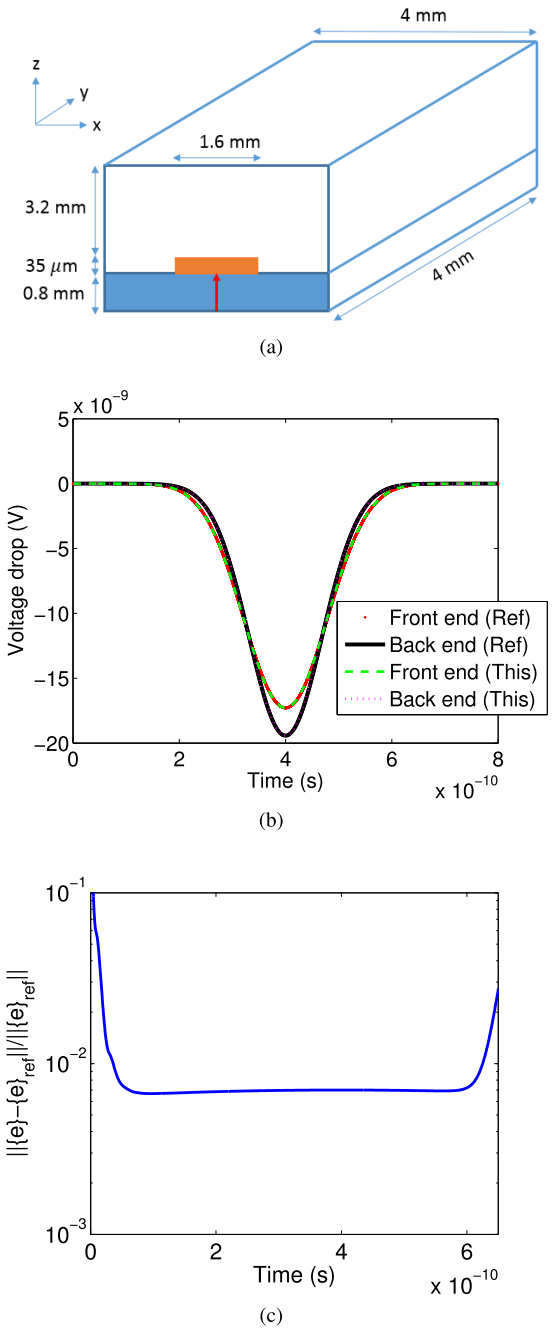

Fig. 7. Microstrip line with fine features. (a) Structure. (b) Voltages at two ports. (c) Entire solution error in comparison with reference FDTD solutions.

respectively. The total number of **E** unknowns in this structure is 4653. Due to the small space step to capture the skin effects, a time step of 5.0×10^{-16} s is required in the conventional FDTD method. In contrast, the proposed method is able to use a time step of 3.6×10^{-13} s. The number of terms kept in (44) is six. In Fig. 7(b), the voltage drops extracted at both near and far ends of the strip line are plotted in comparison with the results obtained from a conventional FDTD method. It is clear that the results of the proposed method agree very well with the reference solutions. The entire solution error at each time instant is evaluated as $\|\{e\} - \{e\}_{\text{FDTD}}\|/\|\{e\}_{\text{FDTD}}\|$, and plotted in Fig. 7(c). Obviously, the proposed method is accurate not only at the two sampled points, but also in the entire computational domain across the entire simulated time window.

In this simulation, 1925 **E** unknowns are involved to assemble $\mathbf{M}_f$. The total time of the proposed method is 208.9699 s, out of which 29.1695 s is used to extract 1317 unstable modes for a prescribed accuracy ϵ=10^{-6}, and 179.8004 s is spent on explicit time marching. In contrast, a conventional FDTD based on (6) requires 813.5459 s to finish the same simulation. The explicit unconditionally stable FDTD method in [18] requires 142.2547 s to extract unstable modes and 259.1829 s to perform time marching. Thus, the proposed method is more efficient, despite the additional computational overhead for solving lossy problems such as the requirement of a series expansion shown in (44).

VI. Conclusion

In this paper, a fast explicit and unconditionally stable FDTD method is developed. It does not require a global eigenvalue solution. In this method, first, we represent the FDTD method into a patch-based single-grid matrix representation, in contrast to a conventional matrix representation that can be viewed as an edge-based dual-grid one. This new representation helps us identify the relationship between unstable eigenmodes and the fine patches. We find that the largest eigenmodes of the system matrix obtained from the entire computational domain can be extracted from the system matrix assembled from the fine patches with controlled accuracy. The larger the contrast ratio of the fine-patch size to the regular one, the more accurate the extracted eigenmodes. This finding can also be used in other research. Based on this theoretical finding, we develop an accurate and fast algorithm for finding unstable modes from fine patches. We then upfront eradicate these unstable modes from the numerical system before performing an explicit time marching. The resultant simulation eliminates the shortcoming of the original FDTD in time step's dependence on space step, without sacrificing the merit of the FDTD in an explicit time marching. The proposed method is also extended to handle general lossy problems where dielectrics and conductors are inhomogeneous and lossy. Numerical experiments including both lossless and lossy problems have demonstrated the accuracy, efficiency, and unconditional stability of the proposed method, by comparing with conventional FDTD as well as the state-of-the-art explicit and unconditionally stable method. The essential idea of this paper is also applicable to other time-domain methods. It is also worth mentioning that although the unstable modes are extracted from fine patches and subsequently removed for a stable simulation, this does not mean that the resultant field solution in the fine patches is zero or has a large error. This is because the stable eigenmodes preserved in the numerical system have their field distributions all over the grid, including both regular and fine patches. These modes are different when there are fine features and when there are not.

References

[1] K. S. Yee, "Numerical solution of initial boundary value problems involving Maxwell's equations in isotropic media," *IEEE Trans. Antennas Propag.*, vol. AP-14, no. 3, pp. 302–307, May 1966.

[2] A. Taflove and S. C. Hagness, *Computational Electrodynamics*, 3rd ed. Norwood, MA, USA: Artech House, 2005.
[3] T. Namiki, "A new FDTD algorithm based on alternating-direction implicit method," *IEEE Trans. Microw. Theory Techn.*, vol. 47, no. 10, pp. 2003–2007, Oct. 1999.
[4] F. Zheng, Z. Chen, and J. Zhang, "A finite-difference time-domain method without the Courant stability conditions," *IEEE Microw. Guided Wave Lett.*, vol. 9, no. 11, pp. 441–443, Nov. 1999.
[5] C. Sun and C. W. Trueman, "Unconditionally stable Crank–Nicolson scheme for solving two-dimensional Maxwell's equations," *Electron. Lett.*, vol. 39, no. 7, pp. 595–597, Apr. 2003.
[6] J. Lee and B. Fornberg, "A split step approach for the 3-D Maxwell's equations," *J. Comput. Appl. Math.*, vol. 158, no. 2, pp. 485–505, 2003.
[7] J. Shibayama, M. Muraki, J. Yamauchi, and H. Nakano, "Efficient implicit FDTD algorithm based on locally one-dimensional scheme," *Electron. Lett.*, vol. 41, no. 19, pp. 1046–1047, Sep. 2005.
[8] V. E. Nascimento, B.-H. V. Borges, and F. L. Teixeira, "Split-field PML implementations for the unconditionally stable LOD-FDTD method," *IEEE Microw. Wireless Compon. Lett.*, vol. 16, no. 7, pp. 398–400, Jul. 2006.
[9] G. Zhao and Q. H. Liu, "The unconditionally stable pseudospectral time-domain (PSTD) method," *IEEE Microw. Wireless Compon. Lett.*, vol. 13, no. 11, pp. 475–477, Nov. 2003.
[10] Y.-K. Chung, T. K. Sarkar, H. J. Baek, and M. Salazar-Palma, "An unconditionally stable scheme for the finite-difference time-domain method," *IEEE Trans. Microw. Theory Techn.*, vol. 51, no. 3, pp. 697–704, Mar. 2003.
[11] Z. Chen, Y.-T. Duan, Y.-R. Zhang, and Y. Yi, "A new efficient algorithm for the unconditionally stable 2-D WLP-FDTD method," *IEEE Trans. Antennas Propag.*, vol. 61, no. 7, pp. 3712–3720, Jul. 2013.
[12] Z.-Y. Huang, L.-H. Shi, B. Chen, and Y.-H. Zhou, "A new unconditionally stable scheme for FDTD method using associated Hermite orthogonal functions," *IEEE Trans. Antennas Propag.*, vol. 62, no. 9, pp. 4804–4809, Sep. 2014.
[13] E. L. Tan, "Fundamental schemes for efficient unconditionally stable implicit finite-difference time-domain methods," *IEEE Trans. Antennas Propag.*, vol. 56, no. 1, pp. 170–177, Jan. 2008.
[14] Q. He and D. Jiao, "An explicit time-domain finite-element method that is unconditionally stable," in *Proc. IEEE Int. Symp. Antennas Propag.*, Jul. 2011, pp. 1–4.
[15] C. Chang and C. D. Sarris, "A spatially filtered finite-difference time-domain scheme with controllable stability beyond the CFL limit: Theory and applications," *IEEE Trans. Microw. Theory Techn.*, vol. 61, no. 3, pp. 351–359, Jan. 2013.
[16] Q. He, H. Gan, and D. Jiao, "Explicit time-domain finite-element method stabilized for an arbitrarily large time step," *IEEE Trans. Antennas Propag.*, vol. 60, no. 11, pp. 5240–5250, Nov. 2012.
[17] M. Gaffar and D. Jiao, "An explicit and unconditionally stable FDTD method for electromagnetic analysis," *IEEE Trans. Microw. Theory Techn.*, vol. 62, no. 11, pp. 2538–2550, Nov. 2014.
[18] M. Gaffar and D. Jiao, "Alternative method for making explicit FDTD unconditionally stable," *IEEE Trans. Microw. Theory Techn.*, vol. 63, no. 12, pp. 4215–4224, Dec. 2015.
[19] J. Yan and D. Jiao, "Explicit and unconditionally stable FDTD method without eigenvalue solutions," in *IEEE MTT-S Int. Microw. Symp. Dig.*, May 2016, pp. 1–4.
[20] R. F. Remis, "On the stability of the finite-difference time-domain method," *J. Comput. Phys.*, vol. 163, no. 1, pp. 249–261, 2000.
[21] M. Gaffar and D. Jiao, "An explicit and unconditionally stable FDTD method for the analysis of general 3-D lossy problems," *IEEE Trans. Antennas Propag.*, vol. 63, no. 9, pp. 4003–4015, Sep. 2015.
[22] J. Lee, D. Chen, V. Balakrishnan, C.-K. Koh, and D. Jiao, "A quadratic eigenvalue solver of linear complexity for 3-D electromagnetics-based analysis of large-scale integrated circuits," *IEEE Trans. Comput.-Aided Des. Integr. Circuits Syst.*, vol. 31, no. 3, pp. 380–390, Mar. 2012.
[23] W. Heinrich, K. Beilenhoff, P. Mezzanotte, and L. Roselli, "Optimum mesh grading for finite-difference method," *IEEE Trans. Microw. Theory Techn.*, vol. 44, no. 9, pp. 1569–1574, Sep. 1996.
[24] L. N. Trefethen, "Group velocity in finite difference schemes," *SIAM Rev.*, vol. 24, no. 2, pp. 113–136, 1982.
[25] J. Yan and D. Jiao, "Fast explicit and unconditionally stable FDTD method for electromagnetic analysis," Ph.D. dissertation, School Elect. Comput. Eng., Purdue Univ., West Lafayette, IN, USA, 2017.
[26] I. G. Zubal, C. R. Harrell, E. O. Smith, Z. Rattner, G. Gindi, and P. B. Hoffer, "Computerized three-dimensional segmented human anatomy," *Med. Phys.*, vol. 21, no. 2, pp. 299–302, 1994.

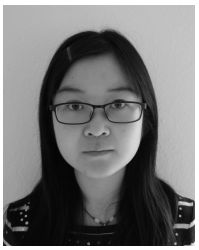

Jin Yan (GS'13) received the B.S. degree in electronic engineering and information science from the University of Science and Technology of China, Hefei, China, in 2012. She is currently pursuing the Ph.D. degree in electrical engineering at Purdue University, West Lafayette, IN, USA.

She is currently with the On-Chip Electromagnetics Group, Purdue University. Her current research interests include computational electromagnetics, high-performance VLSI CAD, and fast and high-capacity numerical methods.

Ms. Yan was a recipient of an Honorable Mention Award of the IEEE International Symposium on Antennas and Propagation in 2015 and the Best Student Paper Award Finalist of the IEEE MTT-S International Microwave Symposium in 2016.

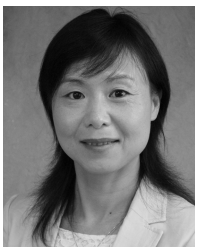

Dan Jiao (M'02–SM'06–F'16) received the Ph.D. degree in electrical engineering from the University of Illinois at Urbana–Champaign, Champaign, IL, USA, in 2001.

She was with the Technology Computer-Aided Design (CAD) Division, Intel Corporation, until 2005, as a Senior CAD Engineer, Staff Engineer, and Senior Staff Engineer. In 2005, she joined the School of Electrical and Computer Engineering, Purdue University, West Lafayette, IN, USA, as an Assistant Professor, where she is currently a Professor. She has authored 3 book chapters and over 260 papers in refereed journals and international conferences. Her current research interests include computational electromagnetics, high-frequency digital, analog, mixed-signal, and RF integrated circuit design and analysis, high-performance VLSI CAD, modeling of microscale and nanoscale circuits, applied electromagnetics, fast and high-capacity numerical methods, fast time-domain analysis, scattering and antenna analysis, RF, microwave, and millimeter-wave circuits, wireless communication, and bioelectromagnetics.

Dr. Jiao has served as the reviewer for many IEEE journals and conferences. She is an Associate Editor of the IEEE TRANSACTIONS ON COMPONENTS, PACKAGING, AND MANUFACTURING TECHNOLOGY. She received the 2013 S. A. Schelkunoff Prize Paper Award of the IEEE Antennas and Propagation Society, which recognizes the Best Paper published in the IEEE TRANSACTIONS ON ANTENNAS AND PROPAGATION during the previous year. She was among the 21 women faculty selected across the country as the 2014–2015 Fellow of Executive Leadership in Academic Technology and Engineering at Drexel, a national leadership program for women in the academic STEM fields. She has been named a University Faculty Scholar by Purdue University since 2013. She was among the 85 engineers selected throughout the nation for the National Academy of Engineering's 2011 U.S. Frontiers of Engineering Symposium. She was a recipient of the 2010 Ruth and Joel Spira Outstanding Teaching Award, the 2008 National Science Foundation CAREER Award, the 2006 Jack and Cathie Kozik Faculty Start-up Award (which recognizes an outstanding new faculty member of the School of Electrical and Computer Engineering, Purdue University), a 2006 Office of Naval Research Award under the Young Investigator Program, the 2004 Best Paper Award presented at the Intel Corporation's annual corporate-wide technology conference (Design and Test Technology Conference) for her work on generic broadband model of high-speed circuits, the 2003 Intel Corporation's Logic Technology Development (LTD) Divisional Achievement Award, the Intel Corporation's Technology CAD Divisional Achievement Award, the 2002 Intel Corporation's Components Research the Intel Hero Award (Intel-wide she was the tenth recipient), the Intel Corporation's LTD Team Quality Award, and the 2000 Raj Mittra Outstanding Research Award presented by the University of Illinois at Urbana–Champaign.